Preparation of zinc oxide with three-dimensionally interconnected macroporous structure through sol-gel method accompanied by phase separation

Xuanming Lu[1] · Kazuyoshi Kanamori[1] · Kazuki Nakanishi[1,2 *]

[1]Department of Chemistry, Graduate School of Science, Kyoto University, Kitashirakawa, Sakyo-ku, Kyoto 606-8502, Japan

[2]Division of Materials Research, Institute of Materials and Systems for Sustainability, Nagoya University, Furo-cho, Chikusa-ku, Nagoya, Aichi 464-8601, Japan

E-mail:dknakanishi@imass.nagoya-u.ac.jp

Abstract

A facile method for the preparation of zinc oxide with three-dimensionally (3D) interconnected macropores has been developed. The Zn-based monolithic gel was obtained using citric acid (CA) as a structure supporter via epoxide-mediated sol-gel method accompanied by phase separation. The size of macropores could be controlled by the ratio of methanol to propylene oxide in the starting solution. The Zn-based gel was heat-treated in air with the purpose of removing the organic components and crystallizing the ZnO, finally resulted in ZnO (purity > 90 %, with negligible carbon contents) with 3D interconnected macropores and open nanoscale network. The influence of the starting solvent composition on the Zn-based gel morphologies has been examined and discussed based on the chemical compatibility of Zn-CA complex with other components.

Keywords Zinc oxide; 3D interconnected macropores; Sol-gel; Phase separation;

1. Introduction

Metal oxides (MOs) have been utilized by human beings for a long time in their history. Many kinds of MOs in modern technology play indispensable roles in the fields of catalyst, energy, environment, and so on. However, as the natural abundance is in general limited for major useful elements, functional materials have been developed in the direction of reducing the amount of raw materials required per device. With the progress of in depth understanding of the structure-property relationships, MOs have been designed from traditional bulk form into those with new structures to improve their existing performances or render them new properties.[1-4] For porous materials, efforts have been made to improve the efficiency of accommodating external substance to be interacted with active sites embedded in the materials. Multiscale porous structure is a good example, in which the nm-scale pores contribute to enlarge the available surface area, while the μm-scale pores provide the materials with high accessibility to such an active surface.

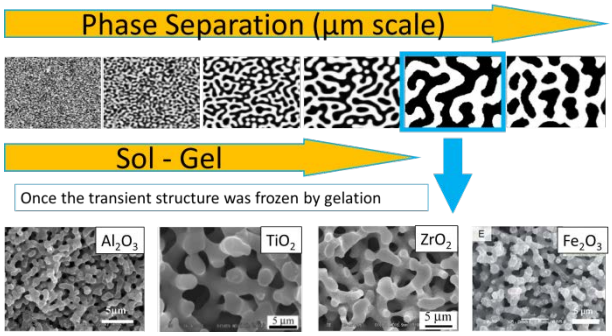

Scheme 1 Synthetic strategy based on sol-gel transition accompanied by phase separation. (Al_2O_3; [8] TiO_2; [9] ZrO_2; [10] Fe_2O_3; [11])

Recently, the synthesis of MOs with multiscale porosities has been abundantly reported.[5-7] Among them, the structure with three-dimensionally (3D) interconnected macropores (μm-scale) and open nanoscale network has been realized successfully in several MOs through sol-gel method accompanied by phase separation.[8-11] Sol-gel has been considered as a “bottom-up” approach to obtain a continuous solid network with nanopores by forced hydrolysis and polycondensation of hydrated metal cations. The interconnected macropores in μm-scale can be obtained by controlling two competitive processes, gelation and phase separation (Scheme 1),

without using any templates which physically leave unoccupied spaces in the resultant material structure. However, there is a limited number of report on successful preparation of pure divalent metal oxides based on this strategy. The main reason is that the hydrolysis and polycondensation is unfavored for low-valence cations due to their low acidity.[12, 13] The slow hydrolysis/polycondensation tends to lead to precipitation rather than homogeneous gelation. Nevertheless, in our previous studies, Ni-based[14] and Cu-based[15] materials with 3D interconnected macroporous structure had been prepared using poly(acrylic acid) (HPAA) and polyacrylamide (PAAm), respectively, as structure supporters. Since the organic components account for predominant fraction in the skeleton, the crystallization of these oxides without losing their network structure required heat-treatment in a reducing atmosphere. As a result, considerable amount of carbon remains in the network, and then pure metal oxides with 3D interconnected macroporous structure could not be obtained.

Among the divalent MOs, zinc oxide (ZnO) has attracted a great deal of attention, scientifically and technologically, owing to its direct wide band gap of 3.37 eV. It has been extensively studied and applied in the fields of piezoelectrics[16], photocatalyst[17], gas sensor[18], transparent electrodes[19], and UV photodetector.[20, 21] ZnO nanorods[22], nanowires[20, 22], nanosheets[18, 23], and nanotetrapods[21] have been abundantly synthesized, where the majority of materials shapes are classified into one- or two-dimensions except for nanotetrapods.

Some researchers tried to synthesize ZnO with 3D continuous porous structure by a templating method.[24, 25] However, there is still limited number of reports on synthesis of ZnO with 3D continuous network structure, not to mention preparation without template. Nasiri and co-workers synthesized ZnO nanoparticle networks by liquid-fed spray flame synthesis and aerosol deposition.[26] Wang and co-workers synthesized 3D porous ZnO foam structures by a rapid combustion of ethylene glycol solution of zinc nitrate.[18] The pores were produced by a large quantity of gases generated in the combustion process, making controls over pore structure and reproducible synthesis very difficult. Dilger and co-workers prepared ZnO with multiple porosities by ultrafast temperature gradient chemical gas-phase synthesis.[27] In their works, an uncommon organic precursor, methylzinc methoxyethoxide, was employed; the process required a sophisticated gas phase reactor. Unlike other transition metal oxides, such as TiO_2, ZrO_2, and Fe_2O_3, ZnO exhibits difficulty to construct a well-defined 3D interconnected structure because of

rapid crystallization of ZnO and $Zn(OH)_2$ in an aqueous solvent.[21, 23] This is one of the reason why the preceding reports are mostly limited to low dimensional structures. It is, therefore, still a challenge to prepare pure zinc oxide with 3D interconnected network structure.

In this work, we present a facile method to synthesize 3D interconnected macroporous ZnO through sol-gel process accompanied by phase separation, and subsequent heat-treatment. The difficulty of gelation can be perfectly overcome by adopting tri-carboxylic acid, citric acid (CA), as ligands to bridge between Zn-based species.[28,29] Propylene oxide (PO), as an acid scavenger was used to raise the solution pH uniformly by a ring-opening reaction, which allowed gelation. On the other hand, PO as a poor solvent was distributed to the solvent phase against Zn-CA species rich phase in the phase-separation process. The size of macropores could be controlled by the concentration of PO in the starting solvents. In contrast to the cases of Ni-HPAA-system and Cu-PAAm-system mentioned above, by the heat-treatment in air, the resultant gels gave pure crystalline metal oxide without losing their 3D interconnected network structures.

2. Experimental

2.1 Starting materials

Zinc nitrate hexahydrate ($Zn(NO_3)_2 \cdot 6H_2O$, > 98 %), citric acid, propylene oxide, and 1,2-epoxybutan (EB) were purchased from Sigma-Aldrich Japan. Methanol (MeOH, > 99 %), and 2-propanol (IPA, > 99 %), were purchased from Kishida Chemical Co., Ltd. (Japan). All the agents were used without further purification.

2.2 Preparation of Zn-based gels

The typical synthesis procedure for the monolithic Zn-based gel is as follows. 2 mmol of $Zn(NO_3)_2 \cdot 6H_2O$ were dissolved in a predetermined amount of methanol in a 9 mL glass bottle. Then 1 mmol of citric acid was added to the zinc nitrate solution under stirring. The solution was cooled in an ice-water bath after the citric acid was dissolved completely. A predetermined amount of propylene oxide was injected into the solution in the ice-water bath under stirring,

followed by stirring for 10 sec. The mixed solution was tightly sealed and placed in a refrigerator at 4~5 ℃ for gelation. A white opaque resultant gel was kept in the refrigerator for 30 min and subsequently aged at 25 ℃ for 24 h. After the solvent exchange with 2-propanol at 60 ℃ for 3 times, the gel was dried in a container covered by a lid with small holes at 40 ℃. The crystalline ZnO with 3D interconnected macropores was obtained by heat-treatment in air. The samples were heated, firstly, from room temperature to 300 ℃ with the heating rate of 1 ℃/min and kept at 300 ℃ for 2 h. Secondly, the samples were slowly heated from 300 ℃ to 310 ℃ with the heating rate of 0.5 ℃/min and kept at 310 ℃ for 2 h. Thirdly, the samples were heated from 310 ℃ to the target temperatures (320, 360, or 400 ℃) with the heating rate of 0.5 ℃/min and kept at the target temperature for 2 h. Finally, the samples were cooled with the rate of 1 ℃/min down to 100 ℃ and left at the room temperature.

2.3 Characterization

The structures of resultant gels in the micrometer range and the chemical compositions were examined by a scanning electron microscope equipped with energy dispersive X-ray spectroscope (SEM-EDS, JSM-6060S, JEOL, Japan). The macropore size distributions of gels were determined by a mercury porosimeteter (Autopore IV 9505, Shimadzu Co., Japan). Nitrogen adsorption-desorption isotherms were obtained using BELSORP-mini II (Microtrac BEL, Japan). Before the measurements, samples were degassed under vacuum at 120 ℃. Specific surface area was calculated using the Brunauar-Emmett-Teller (BET) method, and the pore size distribution in the mesopore regime was calculated from the adsorption branch of the isotherm using the Barrett-Joyner-Halenda (BJH) method.

Thermal evolutions of the as-dried gels were measured by thermogravimetry-differential thermal analyzer (TG-DTA; Thermo plus EVO, TG-DTA 8120, Rigaku Co., Japan), at a heating rate of 1 ℃ min^{-1}, with a continuous air supply at 100 mL min^{-1}. The Fourier transform infrared (FT-IR) spectra were obtained by an FT-IR spectrometer (IRAffinity-1, Shimadzu Co., Japan) using KBr technique. Crystalline phases of the samples were investigated by an X-ray diffractometer (XRD; RINT Ultima III, Rigaku Co., Japan) using Cu Kα (λ = 0.154 nm) as an incident beam.

3. Results and discussion

3.1 Zn-based as-dried gels

Table 1 The phase separation time t_{ps} and gelation time t_g of samples prepared by varied ratio of methanol to propylene oxide

sample	MeOH/PO (mL/mL)	t_{ps} / min	t_g / min
a	0.8/0.6	-	130
b	0.7/0.7	31	50
c	0.6/0.8	17	30
d	0.5/0.9	11	15
e	0.4/1.0	5	10
f	0.3/1.1	3	6

No macroscopic gelation has been observed in the absence of CA. The time of phase separation (denoted as t_{ps}) and the time of gelation (denoted as t_g) are listed in Table 1. Here, t_{ps} was recorded as the time when the transparency of the system started to decrease; t_g was recorded when the system lost its fluidity. With an increasing concentration of PO in the solution, the t_{ps} and t_g became shorter. PO acted as an acid scavenger to raise solution pH through an irreversible ring-opening reaction with nitrate (Eq. 1).

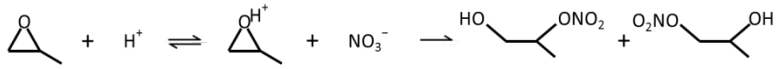

(1)

In the present experimental condition, higher concentration of PO simply resulted in quicker raise of the solution pH and then earlier gelation. In the sample (b)-(f), the solutions exhibited fluidity when they turned white and opaque. Since the emergence of opaqueness can be ascribed to the onset of phase separation, the phase separation occurred earlier than gelation in these samples. Figure 1 shows the SEM images of as-dried gels prepared with varied volume ratio of MeOH to PO. 3D interconnected macropores are observed except sample (a). The size of macropores increased and the skeleton became thinner relative to the adjacent pore spaces with an increase of the concentration of added PO. The morphology with no macropores was observed in sample (a). The detailed analysis of the effects of onset of phase separation and gelation time is described in the case of pure silica in the literature.[30]

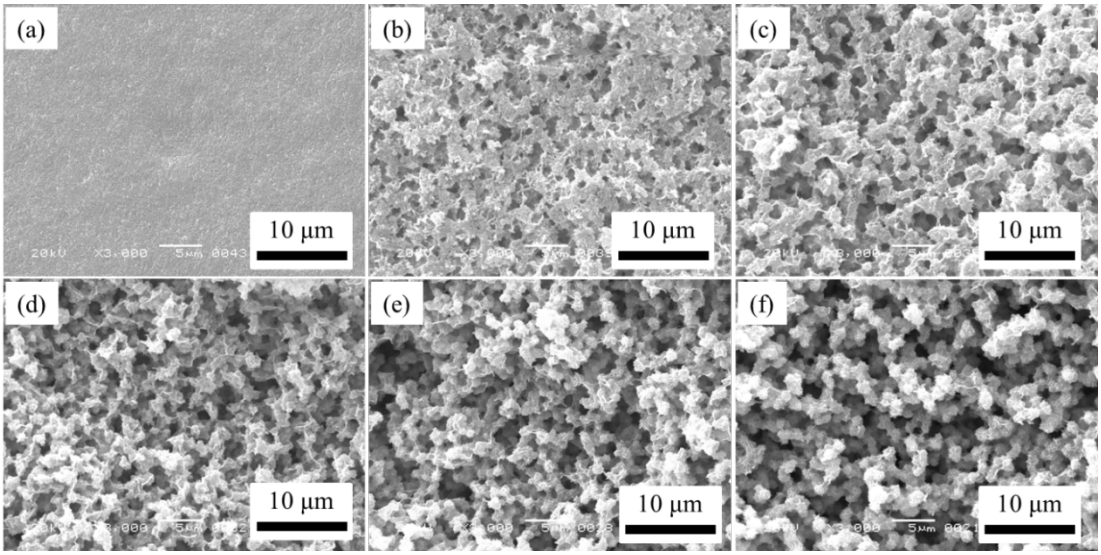

Fig. 1 SEM images of as-dried gels prepared with varied volume ratio of methanol to propylene oxide (MeOH/PO). (a) 0.8/0.6; (b) 0.7/0.7; (c) 0.6/0.8; (d) 0.5/0.9; (e) 0.4/1.0; (f) 0.3/1.1;

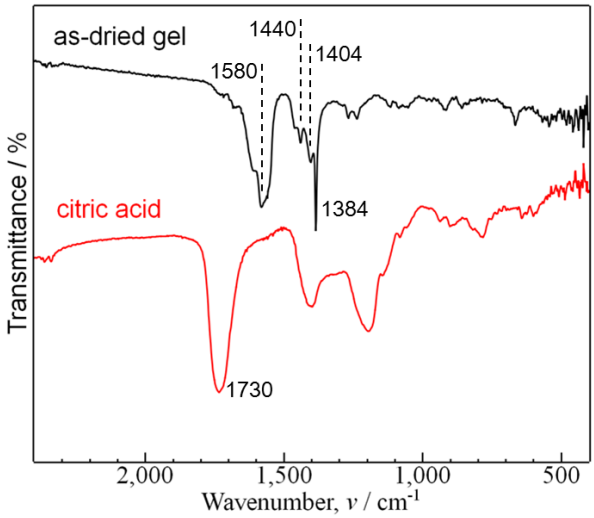

Fig. 2 FT-IR spectra of as-dried gel (sample (c)) and citric acid

Sample (c) was used for the examination by FT-IR spectrometer and TG-DTA. As illustrated in Fig. 2, the sharp absorption peak at 1384 cm^{-1} in the spectrum of as-dried gel is ascribed to nitrate ions.[31-33] The antisymmetric stretching vibrations ν_{as}(COO) appear at around 1580 cm^{-1}, whereas the corresponding symmetric stretching vibrations ν_{s}(COO) appear at 1440 cm^{-1} and 1404 cm^{-1}.[28, 32, 34] The antisymmetric ν_{as}(COO) stretching mode in sample (c) is shifted to lower wavenumber compared to that of free citric acid, indicating that the carboxy groups have coordinated with zinc ions. The wavenumber difference $\Delta\nu = \nu_{as} - \nu_{s}$ ranged from 140 cm^{-1} to 176 cm^{-1} for sample (c) suggesting that the carboxy groups are coordinated to zinc ion in bidentate

bridging mode and/or monodentate mode.[32, 35-37] In addition, the hydroxy group in the citric acid is also coordinated with zinc ion to form a five- and six-membered chelate ring.[34, 38] The absence of typical absorption bands corresponding to undissociated carboxylic acid groups at 1730 cm^{-1} also indicates that the majority of carboxy groups had coordinated to the zinc ions. There is no strong absorption at low wavenumber (around 500 cm^{-1}) that indicated the bonding of Zn-O-Zn is sparse in the sample.[39]

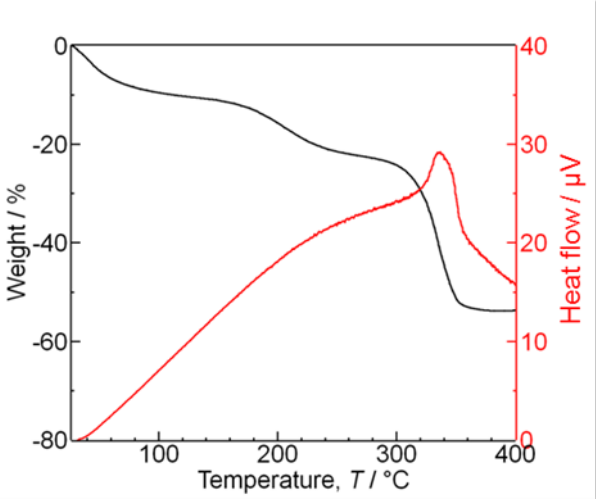

Fig. 3 TG-DTA curves of as-dried gel (sample (c))

According to TG-DTA curves (Fig. 3), about 24 % of weight loss was observed at the temperature range below 300 °C, which is attributed to dehydration of physically adsorbed water and crystalline water. About 30 % of weight loss at the temperature range from 300 °C to 360 °C accompanied by an exothermic peak is ascribed to the combustion of organic component. The amorphous structures transformed to wurtzite ZnO in this temperature range, which will be further discussed in the section 3.4.

3.2 Sol-gel process and phase separation

The results of FT-IR and TG-DTA indicate that the gel phase contained Zn-CA species as major components. The absence of the strong absorption band at low wavenumber in FT-IR spectrum implies that the polycondensation of Zn hydrated cation was limited. Thus, the gelation is

regarded as a result of the coordination between zinc ion and citric acid, rather than hydrolysis-condensation of zinc cation itself.

The phase separation tendency can be estimated by the Flory-Huggins formulation (Eq. 2).

$$\Delta G \propto RT\left(\frac{\Phi_1}{P_1}\ln\Phi_1 + \frac{\Phi_2}{P_2}\ln\Phi_2 + \chi_{12}\Phi_1\Phi_2\right) \qquad (2)$$

Where ΔG is Gibbs free energy change of mixing, R is the gas constant, T is the temperature, Φ_i and P_i are the volume fraction and the degree of polymerization of component i (i = 1 or 2), respectively, and χ_{12} is the interaction parameter between component 1 and component 2. The former two terms in the bracket express the entropic contribution, and the last term expresses the enthalpic contribution. When ΔG becomes positive, the system become unstable, and then phase separation occurs. In the present work, the system can be simplified as a pseudobinary system, in which one is Zn-CA rich phase (denoted as component 1), and the other is the solvent phase (denoted as component 2). The multiple coordinations of CA to Zn ion increases P_1, while P_2 remains unity. At the same time, the preferred coordination of CA to Zn ion in place of individually hydrated species should lower the solubility of Zn-CA complex in the solvent. Consequently, the enthalpic contribution becomes more positive (repulsive). The positive enthalpic contribution will be affected by the concentration of PO in the solvent composition. Since the PO is regarded as a poor solvent preferentially distributed to the solvent phase in present system (as further discussed below), the positive deviation of χ_{12} will occur with an increase of PO concentration. The SEM results indicate that the enthalpic contribution became positive enough to make to the Gibbs free energy positive, around the volume ratio of MeOH/PO = 0.7/0.7, to induce the phase separation occurred in the course of hydrolysis/polycondensation process.

3.3 Roles of methanol and propylene oxide

As the amount of MeOH was varied at a fixed amount of PO, the volume factions of solid networks and macropores only showed negligible changes (Fig. S1). In other words, the amount of MeOH, in a certain range of MeOH/PO ratio, has a minor effect on the volume factions of gel phase (Zn-CA rich phase) and solvent phase. Thus, the MeOH can be reasonably considered as a co-solvent, which is distributed to both the gel phase and the solvent phase without changing

relative volume fractions of the phases.

In the present system, the amount of PO (8 ~ 15 mmol corresponding to 0.6 ~ 1.1 mL) is much more than the stoichiometric amount against the nitrate (4 mmol) in the starting solution. The coordination of CA to zinc will be dominated by the pH value. In other words, the gelation is dominated by the reaction between PO and nitrate. In all cases, the phase separation occurred earlier than gelation (Table 1). It means that a considerable amount of residual PO were present in the solution when the phase separation occurred. Therefore, we consider PO as the poor solvent. We, however, cannot exclude the possibility that the ring-opening reaction products (nitrooxypropanol) work also as the poor solvent to decrease the compatibility against Zn-CA species. The SEM images (Fig. 1) and the mercury intrusion curves (Fig. S2) clearly indicate the simultaneous increase in macropore volume and domain size with the concentraion of PO, in reasonable agreement of the interpretation that PO works as a poor solvent against Zn-CA oligomers to promote phase separation and to increase the fraction of the solvent phase.

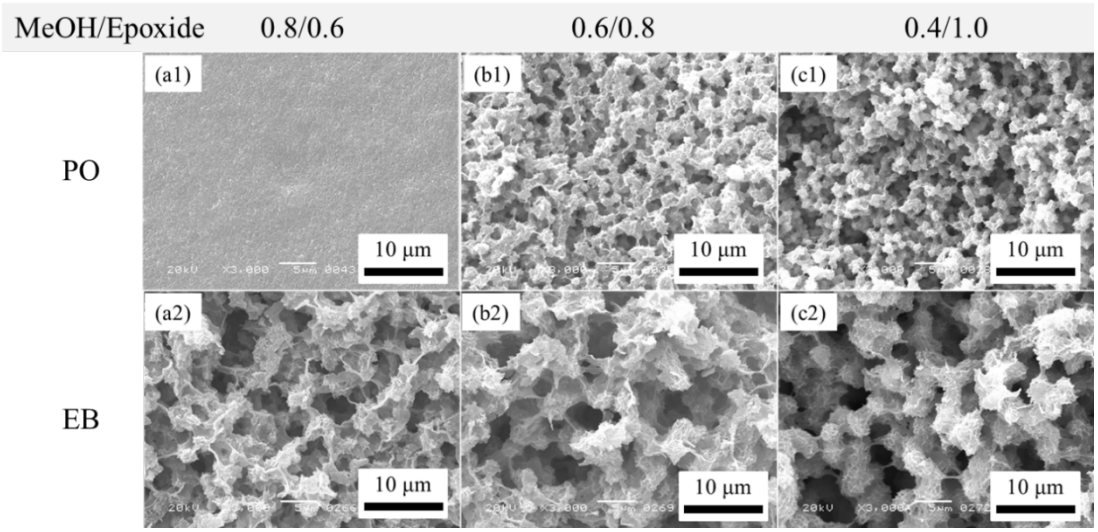

Fig. 4 SEM images of as-dried gels prepared with PO and EB with varied ratios

To further investigate the role of PO played in the phase separation, some samples were prepared using another epoxide, 1,2-epoxybutane (EB), keeping other conditions identical. As a result, when the amounts of epoxides were 0.6 mL (Figs. 4 (a1) and (a2)), the interconnected macroporous structure was observed in the sample prepared by EB, but not in the sample prepared by PO. Moreover, the skeleton became coarser and interconnected macropores became larger as

well when PO was replaced with EB at the amount of 0.8 mL (Figs. 4 (b1) and (b2)) and 1.0 mL (Figs. 4 (c1) and (c2)). EB has relatively lower solubility and lower reactivity than PO in the present system. The lowered compatibility and retarded sol-gel transition are the reasons of morphologies with enhanced phase separation.

3.4 Crystalline ZnO with 3D interconnected macropores

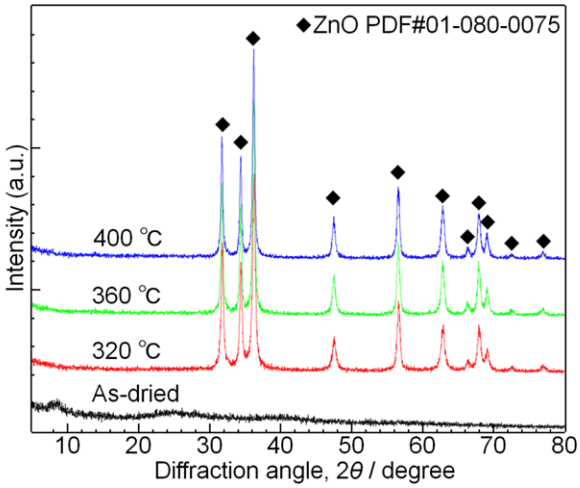

Fig. 5 XRD patterns of samples (sample (c)) before and after heat-treated at varied temperatures

The heat-treatment evolution was studied using sample (c) in table 1. XRD patterns illustrated that wurtzite ZnO without any impurity phase could be obtained after heat-treated in air above 320 °C (Fig. 5). The overall 3D interconnected macroporous structures were preserved after heat-treated in air, naturally accompanied by the isotropic shrinkages (Fig. 6). The result of TG-DTA shows that the majority of organic components were removed when heat-treated above 360 °C. According to the EDS results (Fig. S3), ~7 wt % of carbon was detected in the sample after heat-treated at above 360 °C. This remaining of carbon may be included in ZnO polycrystalline structure so that it is hard to be removed completely, even the heat-treatment temperature up to 500 °C. Nevertheless, it can be claimed that 3D interconnected crystalline ZnO with minor carbon inclusions could be prepared by this method. In contrast to previous works on divalent metal based gels, where organic polymers with amide or carboxy groups were used to support the 3D network structure which was destroyed after the heat-treatment in air.

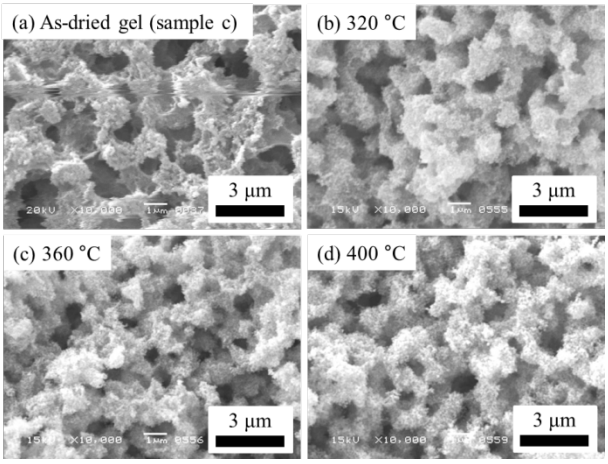

Fig. 6 SEM images of Zn-based as-dried gel before (a) and after heat-treated at varied temperatures (b-d)

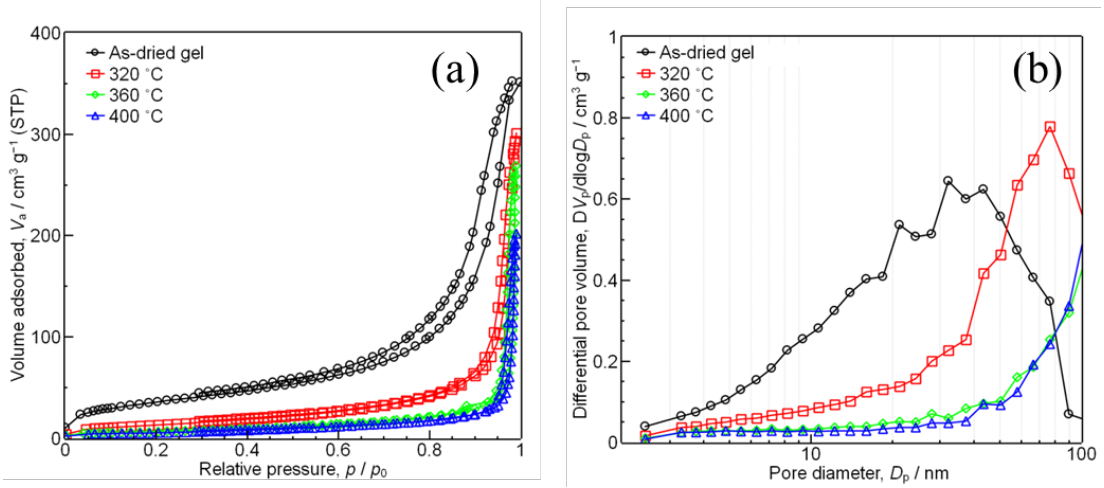

Fig. 7 Nitrogen adsorption/desorption isotherms and corresponding BJH pore size distributions obtained from as-dried samples (sample (c)) before and after heat-treated at varied temperatures

Figures 7a and 7b show the nitrogen adsorption-desorption isotherms and the corresponding pore size distributions, respectively, of the as-dried gels before and after heat-treatment at varied temperatures. All the samples exhibited the isotherms of type IV of the IUPAC classification with relatively small uptakes at lower relative pressures. It indicates that the limited volume of micropores are present in all ZnO samples. Figure 7(b) shows that the pore size distribution shifts to larger size region after the heat treatment. Moreover, the specific surface area and pore volume decreased from 50 to 18 m^2 g^{-1} and 0.46 to 0.31 cm^3 g^{-1}, respectively, with a further increase of the heat-treated temperature from 320 to 400 °C (Table 2). These results are reasonably ascribed to the growth of individual ZnO nanoparticles and their interstitial spaces.

Table 2 BET surface area, S_{BET}, and BJH pore volume, V_p of samples (sample (c)) before and after heat-treated at varied temperatures

sample (c)	S_{BET} m^2 g^{-1}	$V_{p\,(BJH)}$ / cm^3 g^{-1}
As-dried	131	0.53
320 °C	50	0.46
360 °C	20	0.41
400 °C	18	0.31

4. Conclusions

Monolithic ZnO with 3D interconnected macroporous structure has been successfully synthesized via sol-gel process accompanied by phase separation. The difficulty of the gelation of Zn-species has been overcome by coordination with citric acid. The phase separation is induced by the coordination of CA to Zn. The epoxides play duplicated roles: (i) to scavenge protons to raise the solution pH homogeneously to induce the coordination, (ii) to control the phase separation behavior through the solubility of Zn-CA oligomers in the mixed solvent. Epoxides (and/or the ring-opened products) are found to work as poor solvents. Consequently, the 3D macroporous structure can be controlled by the concentrations (and kinds) of epoxides in the starting composition. To the best of our knowledge, this is the first report on the synthesis of ZnO with controllable 3D interconnected macroporous structure without using soft- or hard templates. This study may provide a novel route to synthesize other pure divalent metal oxides with 3D interconnected macropores.

Acknowledgement

This work was supported by Grant-in-Aid for Scientific Research, MEXT, Japan (18H02056), and Incubation Program of Kyoto University. Thanks are due to Dr. Kei Morisato for mercury intrusion measurements, Prof. Hiromitsu Kozuka for his guidance on FT-IR spectra analysis.

References

1. M. Zheng, H. Tang, L. Li, Q. Hu, L. Zhang, H. Xue and H. Pang, *Adv. Mater*., 2018, **5**, 1700592.
2. H. Tan, W. Sun, L. Wang and Q. Yan, *ChemNanoMat*, 2016, **2**, 562-577.
3. G. Zhang, X. Xiao, B. Li, P. Gu, H. Xue and H. Pang, *J. Mater. Chem. A*, 2017, **5**, 8155-8186
4. C. Yuan, H. Wu, Y. Xie and X. Lou, *Angew. Chem. Int. Ed*., 2014, **53**, 1488-1504.
5. D. Grosso, GJ. de AA. Soler-Illia, EL. Crepaldi, B. Charleux and C. Sanchez, *Adv. Funct. Mater.*, 2003, **13**, 37-42.
6. X. Huang, H. Yu, J. Chen, Z. Lu, R. Yazami and H, Hng, *Adv. Mater.*, 2014, **26**, 1296-1303.
7. D. Zhao, J. Qin, L. Zheng and M. Cao, *Chem. Mater.*, 2016, **28**, 4180-4190.
8. Y. Tokudome, K. Fujita, K. Nakanishi, K. Miura and K. Hirao, *Chem. Mater.*, 2007, **19**, 3393-3398.
9. J. Konishi, K. Fujita, K. Nakanishi and K. Hirao, *Chem. Mater.*, 2006, **18**, 6069-6074.
10. J. Konishi, K. Fujita, S. Oiwa, K. Nakanishi and K. Hirao, *Chem. Mater*., 2008, **20**, 2165-2173.
11. Y. Hara, K. Kanamori, K. Morisao, R. Miyamoto and K. Nakanishi, *J. Mater. Chem. A*, 2018, **6**, 9041-9048.
12. U. Schubert and N. Huesing, *Synthesis of Inorganic Materials*, Wiley-VCH, Weinheim, 2012.
13. AE. Gash, TM. Tillotson, JH. Satcher, LW. Hrubesh and RL. Simpson, *J. Non-Cryst. Solids*, 2001, **285**, 22-28.
14. Y. Kido, K. Nakanishi, N. Okumura and K. Kanamori, *Micropor. Mesopor. Mat.*, 2013, **176**, 64-70.
15. S. Fukumoto, K. Nakanishi and K. Kanamori, *New J. Chem*., 2015, **39**, 6771-6777.
16. Z. Wang, *Adv. Funct. Mater.*, 2008, **18**, 3553-3567.
17. N. Daneshvar, D. Salari and AR. Khataee, *J. Photochem. Photobiol. A*, 2004, **162**, 317-322.
18. Z. Jing and J. Zhan, *Adv. Mater*., 2008, **20**, 4547-4551.
19. D. Chen, J. Liang, C. Liu, G. Saldanha, F. Zhao, K. Tong, J. Liu and Q. Pei, *Adv. Funct. Mater.*, 2015, **25**, 7512-7520.
20. C. Soci, A. Zhang, B. Xiang, SA. Dayeh, DPR. Aplin, J. Park, X. Bao, Y. Loand D. Wang, *Nano Lett.*, 2007, **7**, 1003-1009.
21. D. Gedamu, I. Paoulowicz. S. Kaps, O. Lupan, S. Wille, G. Haidarschin, YK. Mishra and R. Adelung, *Adv. Mater*., 2014, **26**, 1541-1550.
22. L. Vayssieres, *Adv. Mater.*, 2003, **15**, 464-466.
23. J. Li, H. Fan and X. Jia, *J. Phys. Chem. C*, 2010, **114**, 14684-14691.
24. E. Kim, Y. Vaynzof, A. Sepe, S. Guldin, M. Scherer, P. Cunha, S. Roth and U. Steiner, *Adv. Funct. Mater.*, 2014, **24**, 863-872.
25. H. Yan, Y. Yang, Z. Fu, B. Yang, L. Xia, S. Fu and F. Li, *Electrochem. Commun.*, 2005, **7**, 1117-1121.
26. N. Nasiri, R. Bo, F. Wang, L. Fu and A. Tricoli, *Adv. Mater*., 2015, **27**, 4336-4343.
27. S. Dilger, C. Lizandara-Pueyo, M. Krumm and S. Polarz, *Adv. Mater*., 2012, **24**, 543-548.
28. B. Chen, X. Wang, S. Zhang, C. Wei and L. Zhang, *J. Porous Mater.*, 2014, **21**, 1035-1039.
29. S.A.M. Lima, F.A. Sigoli, M.R. Davolos, M. Jafelicci Jr., *J. Alloys Compd*., 2002, **334**, 280-284.

30. K. Nakanishi, *J. Porous Mater.*, 1997, **4**, 67-112.
31. M. Liang, O. Deschaume, SV. Patwardhan and CC. Perry, *J. Mater. Chem.*, 2011, **21**, 80-89.
32. G. Wu, L. Wang. DG. Evans and X. Duan, *Eur. J. Inorg. Chem.*, 2006, **2006**, 3185-3196.
33. P. Gerstel, RC. Hoffmann, P. Lipowsky, LPH. Jeurgens, J. Bill and F. Aldinger, *Chem. Mater.*, 2006, **18**, 179-186.
34. D. Chen, Y. Wang, Z. Lin and F. Huang, J. Mol. Struct., 2010, **966**, 59-63.
35. S. Doeuff, M. Henry, C. Sanchez and J. Livage, *J. Non-Cryst. Solids*, 1987, **89**, 206-216.
36. FX. Perrin, V. Nguyen and JL. Vernet, *J. Sol-Gel Sci. Technol.*, 2003, **28**, 205-215.
37. GB. Deacon and RJ. Phillips, *Coord. Chem. Rev.*, 1980, **33**, 227-250.
38. P. Che, D. Fang, D. Zhang, J. Feng, J. Wang, N. Hu and J. Meng, *J. Coord. Chem.*, 2011, **58**, 1581-1588.
39. S. Gago, M. Pillinger, TM. Santos, J. Rocha and IS. Goncalves, *Eur. J. Inorg. Chem.*, 2004, **2004**, 1389-1395.